Automatic Co-registration of Copernicus Time Series via Synchronization

Luigi Barazzetti[1][0000-0002-7859-8677], Andrea Fusiello[2][0000-0003-2963-0316], Marco Gianinetto[1,3][0000-0002-6526-3093], Eleonora Maset[2][0000-0003-3689-1960], Francesco Niccolò Polinelli[1], and Marco Scaioni[1][0000-0003-4058-6176]

[1] ABC Dept. – Politecnico di Milano, Via Ponzio 31 - Milan, Italy
(luigi.barazzetti, marco.gianinetto, francesconiccolo.polinelli, marco.scaioni)@polimi.it
[2] DPIA - Università di Udine, Via Delle Scienze 206 - Udine, Italy
(andrea.fusiello, eleonora.maset)@uniud.it
[3] Institute for Electromagnetic Sensing of the Environment, National Research Council of Italy, Via Bassini 15 - Milan, Italy

Abstract. This paper presents a satellite image co-registration procedure aiming at simultaneously estimating multiple affine transformations between a set of multi-temporal or multi-source satellite images, reducing error accumulation and improving metric precision. The approach is based on *synchronization*, a method that seeks to infer the unknown states of a network of nodes, where only the ratio (or difference) between node pairs can be measured. In our case states represent affine transformations. The proposed method globally combines via synchronization pairwise transformations computed for all the image combinations of the multi-temporal sequence, beyond the traditional image-to-base approach available in remote sensing and GIS packages. Results obtained with Landsat and Sentinel-2 images reveal that the algorithm can be used not only to perform the actual co-registration, but also as a diagnostic tool to evaluate the quality of transformation parameters through a comparison with basic co-registration methods, as well as with global least squares adjustment.

Keywords: Registration, Satellite images, Synchronization, Diagnostic, Copernicus, Sentinel

1 Introduction

Since the first Sentinel launch in 2014, the availability of free and open access satellite images has increased exponentially [11]. Nevertheless, before the release of Level-2 products (i.e., surface reflectance and surface temperature), the enormous amount of information recorded by optical satellites could not be used effectively for geophysical/biophysical analyses. This situation drastically changed in 2018 when the European Space Agency started producing atmospherically-corrected Sentinel-2 images, following the U.S. Geological Survey's best practice for their Landsat missions. Consequently, today the end-users can fully exploit

the increasing potentialities of cloud-based computing platforms for the automatic processing of long time series of images (e.g., Google's Earth Engine). Furthermore, the EU is developing its cloud ecosystem, made of the Copernicus Data and Information Access Services (or DIASes) for commercial applications [10], as well as the free Sentinel Hub for non-commercial use [8].

In this fast-changing scenario, cloud-based tools usually focus on the core methods for data analysis, requiring the user to take care of all the necessary radiometric and geometric pre-processing. Regarding the geometric uncertainties, archived Sentinel-2 images have a 2σ geolocation accuracy of 12.5 m when processed with Ground Control Points (GCPs) [9]. Similarly, Landsat images archived in the Tier 1 collection have a geolocation RMSE of 12 m [25]. Consequently, the time-series analysis or multi-source analysis (e.g., Landsat and Sentinel) might need geocoding refinement to avoid errors due to an insufficient co-registration accuracy. For this reason, many studies were published in the last years about this specific topic [23,18].

The current available strategies for precise *co-registration* (or simply *registration*, or *alignment*) of time-series are illustrated and discussed in [20]. In the case of medium-resolution images, the application of standard pre-processing steps reduces the co-registration process to the computation of a 2D geometric transformation mapping the space of each image into a reference *datum* [16] (a.k.a. *image-to-map* approach). When working with a single image, this task can be accomplished by measuring some GCPs, whose coordinates are retrieved from higher-accuracy digital data or from direct measurement (e.g., by using GNSS positioning). GCPs are then used, together with their corresponding observations in the image, to estimate the parameters of the 2D transformation able to obtain the georeferencing in the given *datum*. An alternative approach for co-registration is based on the *image-to-image* techniques, where images are directly co-registered without external data. While manual measurements of tie-points has been the standard practice since the beginning of Remote Sensing (RS), the development of image matching techniques has allowed to transform this task into an automatic operation (see, e.g., [15]).

When working with time series including several overlapping images, the basic image-to-image co-registration approach – called *image-to-base*[1] – is to select a reference (*base*) image and register all the remaining images to it using basic co-registration processes that works on pairs of images (see, e.g., [13,23]).

On the other hand, some authors have proposed an alternative approach based on the Bundle Block Adjustment (BBA), where the co-registration of a time series is computed by considering tie-points between all overlapping images, and not only w.r.t. the base image [6]. An obvious key feature of BBA is that also images that do not directly share any tie-point with the base image, for example because of some changes in land cover, can be registered together. But, as described in [20], this approach has another feature that becomes very important when tie-points are automatically extracted using image matching algorithms.

[1] The traditional "master-to-slave" terminology has been replaced here with this one, which, albeit not standard, fulfill politically correctness requirements.

Since also robust matching techniques may leave behind wrong observations, the redundancy of tie-points that are used within a BBA can be exploited for a more efficient detection and rejection of errors, according to the theory of *reliability* that has been widely investigated in Geodesy [12]. Such an operational workflow is recommended where many images must be aligned in an automatic way. In this case, the redundancy of tie-points is used to control the quality of the final results.

In this work, an alternative procedure for solving the global co-registration problem called *synchronization* (see Section 3) is presented and compared against Multi-Image Robust Alignment (MIRA), a global least squares adjustment approach that was presented in [20]. The effort of developing an alternative technique to solve for the BBA has multiple aims. First of all, to see whether some cases of failures in the co-registration (e.g., due to the low number or poor distribution of tie-points) can be overcome. Second, the look for a more efficient approach under computational point-of-view. Indeed, when working with massive data sets (hundreds of images in the time series) and with thousands of tie-points, the computational burden of the traditional least squares adjustment may be too much time-consuming also for modern workstations and cloud computing. Third, the availability of two independent approaches for the co-registration of images can be used for mutual validation of the results. This aspect, together with the application of the reliability analysis, is expected to enforce the controllability of the final co-registration.

2 Multi-Image Robust Alignment

Multi-Image Robust Alignment (MIRA) is a global least squares adjustment approach that was presented in [20] with the aim to provide a fully automatic pipeline for the geometric co-registration of satellite time series with sub-pixel accuracy, based on the least squares solution of a system of parametric equations. The method does not depend on external information or user interaction and addresses the following requirements:

- Generic applicability to multi-sensor time series of satellite images;
- Robustness against illumination geometry, atmospheric conditions, land cover changes, image quality, and spatial resolution; and
- Possibility to be easily integrated into existing (RS) processing pipelines.

MIRA is composed of several sequential steps, the first one being keypoint extraction via a SIFT-like approach (found also in [24]). More in detail, the keypoint detector is the one proposed by [17], where blobs with associated scale levels are detected from scale-space extrema of the scale-normalized Laplacian. As for the descriptor, MIRA implements a 128-dimensional radial descriptor, based on the accumulated response of steerable derivative filters.

To detect pairwise matches, a nearest neighbor approach is applied, followed by a robust method based on M-estimator SAmple Consensus (MSAC) to estimate 2D transformations between pairs of images. Finally, a base image is chosen

and an affine transformation able to map each image to the base one is computed with a global least squares adjustment strategy, as described in [6]. In short, each tie-point provides two linear equations where the unknowns are the parameters of the affine transformation of the images. The resulting over-constrained linear system is solved with least squares fitting.

3 Image Registration via Synchronization

In this section, we introduce the global approach known as *synchronization*, that can be applied to image co-registration.

Given a network of nodes (or a graph), where each node is characterized by an unknown state and pairs of nodes connected by an edge can measure the ratio (or difference) between their states, the goal of synchronization [22] is to recover the unknown states from the pairwise measures.

As an example, one can think of topographic levelling as a synchronization problem, where absolute height is the state, differences in elevation between pairs of points are measured, and one wants to retrieve the height of each point.

Mathematically, states are represented by elements of a group Σ. Different instantiations of Σ lead to different variants of the synchronization problem. Among them, it is worth citing the special linear group $SL(d)$ for *homograpy synchronization* [21] and the General Affine group $GA(d)$ for *affine matrix synchronization* [7], where d denotes the dimension, two in our case.

Thanks to the formalism of synchronization, several photogrammetric and computer vision problems [4] can be addressed without relying on features or points, since the problem is formulated in frame space, or, more abstractly, in a group [2]. In [19], e.g., the image mosaicking problem is solved exploiting homography synchronization to align and stitch multiple images and affine synchronization to compute global color corrections. In this paper, the attention is focused on synchronization over $GA(2)$, for multi-temporal or multi-source satellite images are registered applying affine transformations.

In order to formally define the problem and its solution, let $*$ denote the operation in the group Σ. Suppose that the relations between the index pairs $(i, j) \subseteq \{1, .., n\}$ x $\{1, .., n\}$ are known, and refer to them as z_{ij}. *Synchronization* can be formulated as the problem of recovering $x_i \in \Sigma$ for $i = 1, .., n$ such that the following *consistency constraint* is satisfied

$$z_{ij} = x_i * x_j^{-1}. \tag{1}$$

The solution is defined up to a global (right) product with any group element, i.e., if $x_i \in \Sigma$ satisfies (1) then also $x_i * y$ satisfies (1) for any (fixed) $y \in \Sigma$.

Pairwise measures are usually noisy, so the consistency constraint cannot be satisfied exactly. Thus, we search the solution that minimizes the *consistency error*:

$$\epsilon(x_1, x_2, .., x_n) = \sum_{(i,j)} \delta(z_{ij}, x_i * x_j^{-1}) \tag{2}$$

where $\delta : \Sigma \times \Sigma \to \mathbb{R}^+$ is a metric function for Σ [3].

3.1 Synchronization over $(GL(d), \cdot)$

Let us first consider the synchronization problem over the General Linear group $GL(d)$, which is the set of all $d \times d$ invertible matrices, where the group operation $*$ is matrix multiplication and the identity element is I_d. Let $X_i \in \mathbb{R}^{d\times d}$ and $Z_{ij} \in \mathbb{R}^{d\times d}$ denote the matrix representations of $x_i \in \Sigma$ and $z_{ij} \in \Sigma$, respectively. Using this notation, Equation (1) can be rewritten as $Z_{ij} = X_i X_j^{-1}$.

Let us collect the unknown group elements and all the measures in two matrices $X \in \mathbb{R}^{dn\times d}$ and $Z \in \mathbb{R}^{dn\times dn}$ respectively, which are composed of $d \times d$ blocks:

$$X = \begin{bmatrix} X_1 \\ X_2 \\ \dots \\ X_n \end{bmatrix}, \quad Z = \begin{bmatrix} I_d & Z_{12} & \dots & Z_{1n} \\ Z_{21} & I_d & \dots & Z_{2n} \\ \dots & & & \dots \\ Z_{n1} & Z_{n2} & \dots & I_d \end{bmatrix}. \tag{3}$$

If not all the pairwise measures Z_{ij} are available, the input matrix becomes $Z_A := Z \odot (A \otimes \mathbf{1}_{d\times d})$, where $\odot$ denotes the Hadamard product, A is the adjacency matrix, $\mathbf{1}_{d\times d}$ represents a $d \times d$ matrix filled by ones and the Kronecker product with $\mathbf{1}_{d\times d}$ is required to match the block structure of the measures. The $n \times n$ adjacency matrix is constructed as follows: $A_{ij} = 1$ if the pairwise measure Z_{ij} exists, $A_{ij} = 0$ otherwise. Accordingly, the consistency constraint writes

$$Z_A = (XX^{-\flat}) \odot (A \otimes \mathbf{1}_{d\times d}) \tag{4}$$

where $X^{-\flat} \in \mathbb{R}^{d\times dn}$ denotes the block-matrix containing the inverse of each $d \times d$ block of X.

It can be shown [1] that the following relation holds

$$Z_A X = (D \otimes I_d)X \tag{5}$$

where D is the degree matrix defined as $D = \mathrm{diag}(A\mathbf{1}_{n\times 1})$. Thus, the eigenvectors of $(D \otimes I_d)^{-1} Z_A$ corresponding to the d largest eigenvalues represent an estimate of X. This is also known as the *spectral solution*.

3.2 Synchronization over $GA(d)$

The previously described formulation allows us to easily retrieve the solution also for the synchronization over the General Affine group $GA(d)$. This is the set of invertible affine transformations in d-space, which admits a matrix representation through $(d+1) \times (d+1)$ matrices

$$GA(d) = \left\{ \begin{bmatrix} M & \mathbf{v} \\ \mathbf{0}' & 1 \end{bmatrix}, \ s.t.\ M \in \mathbb{R}^{d\times d}, \mathbf{v} \in \mathbb{R}^d \right\}. \tag{6}$$

$GA(d)$ is a subgroup of $GL(d+1)$, therefore, following Equation 5, the synchronization problem can be solved by computing the top $d+1$ eigenvectors of $(D \otimes I_{d+1})^{-1} Z_A$. Since this approach leads to an algebraic solution, it does

not enforce constraints that matrices in $GA(d)$ should satisfy. Going into detail, the output matrix U will not have vector $[\mathbf{0}_{1\times d}\ 1]$ in rows multiple of $d+1$, in general. In order to obtain X from U, one must choose a different basis for the resulting eigenvectors that satisfies such constraint. This can be obtained by solving a linear system of equations, as explained in [5].

To solve the problem of satellite images co-registration, in this work we apply synchronization over $GA(2)$ to convert pairwise affine transformations into global ones. In this way, all transformations between overlapping images are considered simultaneously, minimizing the errors among the whole set of images.

The method is also attractive for its simplicity, as it enjoys an easy and compact Matlab implementation[2]. Moreover, it requires only to store pairwise transformation parameters, with benefits in terms of memory footprint and computing time when compared to other global methods such as MIRA, that relies on the tie-points extracted during the matching phase.

4 Experiments and Results

The novel approach based on affine synchronization (henceforth dubbed AS) is compared with traditional image-to-base approach using the MIRA solution [20] as the baseline.

These approaches were tested with sets of data imaged on different locations, in different seasons and/or years, with different illumination, land cover and cloud coverage as well as different sensors. The common stages of keypoints extraction and matching were performed using the Satellite Automatic Multi-Image Registration (SAMIR) software [14].

4.1 Dataset Sevilla

The Sevilla dataset captures a typical Mediterranean landscape, with flat and hilly topography. All the image tiles were downloaded from Sentinel Hub (https://www.sentinel-hub.com) as already geocoded to the UTM zone 29 N – WGS84 (EPSG:32629) reference system and have a footprint of 110 km x 110 km. More specifically, the dataset Sevilla is made up of 5 images: 4 Sentinel-2/MSI cloud-free images collected over Sevilla (Spain) on 27-APR-2019 (image S2-0), 26-JUN-2019 (image S2-1), 09-SEP-2019 (image S2-2), and 18-NOV-2019 (image S2-3); and 1 additional cloudy Sentinel-2/MSI image collected over Sevilla on 20-AUG-2019 (S2-4). Image co-registration was carried out by using the image acquired on 27-APR-2019 (i.e., S2-0) as base image.

As a first test to validate the co-registration algorithms, only the cloud-free images were taken into account. Fig. 1 shows the location of the extracted tie-points: one can notice that the spatial distribution is not homogeneous over the images and most of them are detected in urban areas, which have a better texture.

[2] Code available at http://www.dpia.uniud.it/fusiello/demo/acs/

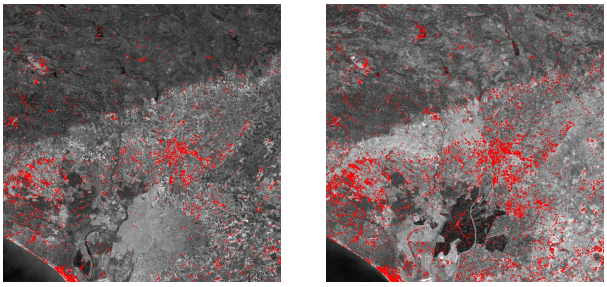

S2-0 S2-1

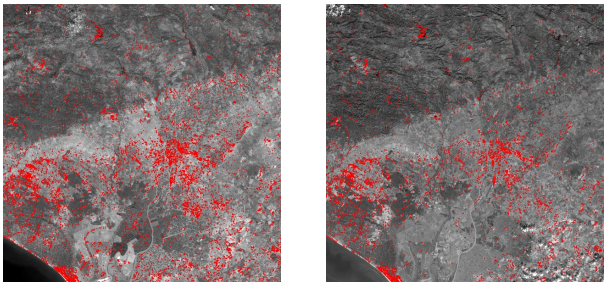

S2-2 S2-3

Fig. 1: Tie-points for the cloud-free images acquired over Sevilla.

The number of tie-points and their distribution was very good for all image combinations, therefore similar parameters were found for the affine transformations computed using different strategies. The number of matched tie-points is always larger than 6,000 for all image combinations (see Tab. 1). Adding more points would make no sense for they tend to fall in already populated areas.

Taking MIRA as the gold standard method, we performed a comparison with the other two co-registration approaches, namely image-to-base and AS, taking the translation error:

$$\Delta T = \sqrt{(T_x^{\mathrm{MIRA}} - T_x^{\mathrm{AS}})^2 + \left(T_y^{\mathrm{MIRA}} - T_y^{\mathrm{AS}}\right)^2} \tag{7}$$

as a figure of merit. We use translation because scale and rotation errors have been found to be negligible, and translations in pixels can be easily related to the error in metric units knowing the ground sampling distance (GSD).

For this first dataset, differences between tested methods are very small: the mean value of ΔT, averaged on the three images, is 0.027 pixel ($\sigma = 0.014$ pixel) for image-to-base vs MIRA and 0.017 pixel ($\sigma = 0.016$ pixel) for AS vs MIRA. This test confirms that the different co-registration algorithms provide the same transformation parameters when a good point distribution can be achieved on all the images of the dataset. It also proves the correctness of the algorithms, and it demonstrates that in the case of few images with a very good overlap with the base, a simple image-to-base approach is sufficient.

Fig. 2 shows the keypoints extracted on the cloudy image S2-4, when introduced in the process. As expected, no keypoints were matched inside the areas covered by clouds.

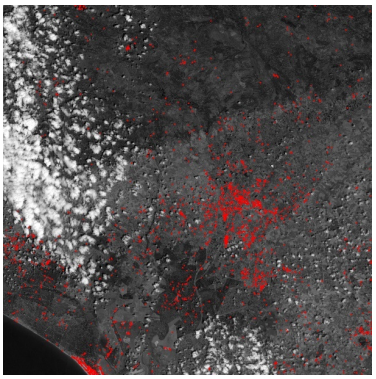

Fig. 2: Cloudy Sentinel-2/MSI image S2-4.

The inclusion of a new image should not affect pairwise matching of the previous images, nevertheless, the process is not repeatable due to random component inside MSAC. To overcome this issue, we did not perform again the matching step but just updated the tie-points with the new combinations including S2-4. Tab. 1 clearly shows that image matching involving S2-4 have a significant smaller number of keypoints.

Table 1: Matched points, including the additional cloudy image.

	S2-0	**S2-1**	**S2-2**	**S2-3**	**S2-4**
S2-0	0	8,072	7,864	6,142	**2,898**
S2-1	8,072	0	22,430	9,316	**5,028**
S2-2	7,864	22,430	0	11,126	**4,476**
S2-3	6,142	9,316	11,126	0	**2,590**
S2-4	**2,898**	**5,028**	**4,476**	**2,590**	**0**

All the co-registration methods performed slightly worse when including the cloudy image. In this case, the mean value of ΔT is 0.058 pixel ($\sigma = 0.038$ pixel) for image-to-base vs MIRA and 0.047 pixel ($\sigma = 0.028$ pixel) for AS vs MIRA.

4.2 Dataset Venice

The Venice dataset features both Sentinel-2/MSI and Landsat-8/OLI images (Fig. 3) and includes flat, hilly and mountain regions, and several urbanized areas. Landsat images were downloaded from Earth Explorer (https://earthexplorer.usgs.gov) as geocoded images in UTM zone 33 N – WGS84 reference system and have a footprint of 185 km × 185 km. Sentinel-2 images were downloaded as described in the Sevilla dataset.

Overall, the dataset is made up of 5 Sentinel-2/MSI images and 5 Landsat-8/OLI images collected over Venice (North-East Italy). Landsat images were collected on 11-JUN-2017 (LS-0), 03-OCT-2019 (LS-1), 10-OCT-2018 (LS-2), 22-NOV-2017 (LS-3), and 20-DEC-2017 (LS-4). Sentinel images were collected on 20-NOV-2017 (S2-5), 15-DEC-2018 (S2-6), 01-NOV-2019 (S2-7), 17-AUG-2018 (S2-8), and 03-JUL-2019 (S2-9).

The co-registration process was carried out using spectral band B03 for both Sentinel-2/MSI (542-578 nm) and Landsat-8/OLI (530-590 nm). We made that choice to make our co-registration pipeline suitable to the processing of any satellite image. Specifically:

- These sectors of the visible spectrum are covered by all the adopted sensors;
- The use of images with similar wavelengths makes easier the detection of corresponding tie-points;
- In the visible spectrum, green has more image contrast because it has a smaller Rayleigh scattering (about 1/4 of total path radiance) compared to blue (about 2/3 of total path radiance).
- In vegetated areas, green has higher contrast (reflectance about 10%-12%) compared to red (reflectance about 4%-5%).

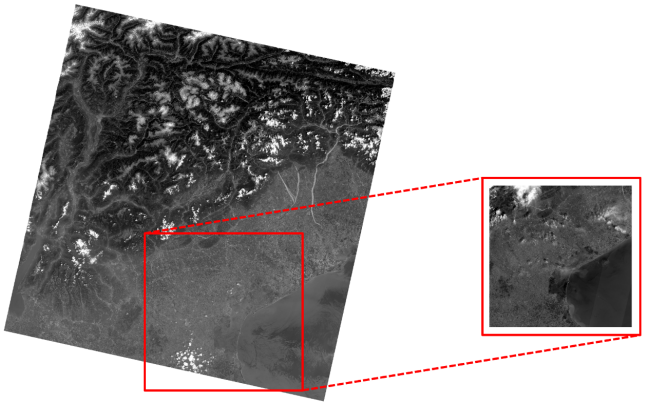

Fig. 3: The different overlap between Sentinel-2/MSI and Landsat-8/OLI.

In this case the use of different cameras, orbits, spatial resolution, and product geocoding accuracy generate larger errors in the registration between mixed

sensors. The correspondence between the Landsat 8 images is relatively good (less than 2 pixel). The results for Sentinel-2 images show larger discrepancies superior to 3 pixels between the different co-registration methods (Fig. 4). Overall, the mean difference between image-to-base and MIRA methods is 1.755±1.506 pixel, while the comparison between AS and MIRA shows slightly lower error values (1.553±1.108 pixel). Such result is worse than previous figures, and unveils that point distribution in the images is not sufficiently good for a reliable co-registration procedure. In this sense, applying 3 different co-registration algorithms (which however are based on the same set of corresponding points) can reveal if the tie-points are sufficiently good to ensure reliable co-registration, which is a fundamental preliminary procedure in remote sensing.

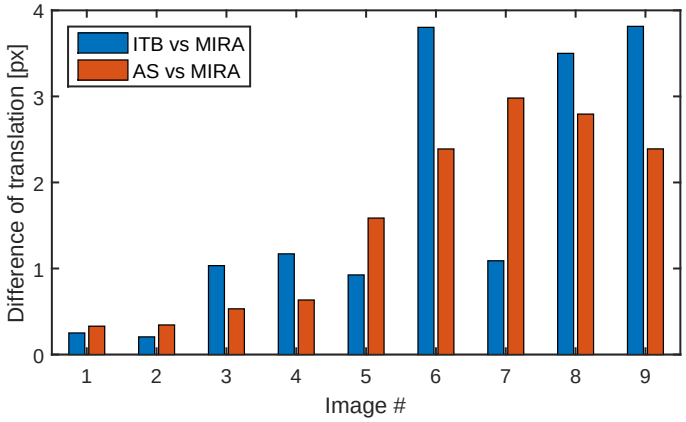

Fig. 4: Results for the Venice dataset. ITB stands for "image-to-base".

4.3 Dataset Po Valley

The last experiment demonstrates the advantage of using MIRA or AS when image-to-base co-registration is not feasible. As a matter of fact, these approaches can successfully register long time series only when the base image has enough matches with the other images. When this is not the case, MIRA and AS can exploit matches extracted between all image pairs, therefore indirectly tying all the images to the base one.

The Po Valley dataset is a typical test for agricultural applications. It includes 9 Landsat-8/OLI images, 13 Sentinel-2A/MSI and 6 Sentinel-2B/MSI images collected from April 2017 to July 2019 in Italy's most fertile land. Satellite images were selected with cloud cover up to 50%, different cloud's spatial distribution and size, to test the robustness against cloud coverage. Besides, the satellite data were not corrected/compensated for the atmospheric effect. That makes the image matching even more challenging.

Unlike the Venice dataset, the image matching was done with the near-infrared spectral bands: band #8a for Sentinel-2 (854-875 nm), and band #5 (850-880 nm) for Landsat-8/OLI. The near-infrared is widely used to monitor farmlands and also partially reduces the impact of the different atmospheric conditions, contrasting crops with different growth stages.

Comparing the parameters estimated via the MIRA method and AS shows that differences are rather small (on average, 0.045 pixel with $\sigma = 0.032$ pixel) and confirms that the two methods provided equivalent results. As mentioned, the comparison does not include the image-to-base strategy which cannot be applied in this scenario for the impossibility to match the base image with all the others images.

5 Conclusion

Synchronization has a wide range of interesting applications [2]. In this paper we applied it to the co-registration of remote sensing images as an alternative to the more traditional image-to-base approach. Both MIRA and AS can overcome the lack of co-registration results when the base image does not share matches with all the remaining images in the dataset. In fact, image-to-base co-registration strategies usually available in remote sensing/GIS software packages cannot automatically complete the co-registration workflow for those images. The use of methods able to handle also matches extracted between other (all, in principle) image pairs can overcome this limitation. Experiments in the paper have shown that a discrepancy between the computed parameters with both AS and MIRA could indicate an unreliable set of matches extracted automatically in the image dataset. Comparing the parameters estimated with both methods can be therefore intended as an additional diagnostic tool able to verify the reliability of the extracted set of tie-points.

References

1. Arie-Nachimson, M., Kovalsky, S.Z., Kemelmacher-Shlizerman, I., Singer, A., Basri, R.: Global motion estimation from point matches. In: Proceedings of the Joint 3DIM/3DPVT Conference: 3D Imaging, Modeling, Processing, Visualization and Transmission (2012)
2. Arrigoni, F., Fusiello, A.: Synchronization problems in computer vision with closed-form solutions. International Journal of Computer Vision **128**(1), 26–52 (2020)
3. Arrigoni, F., Fusiello, A., Rossi, B.: Camera motion from group synchronization. In: Proceedings of the International Conference on 3D Vision (3DV), pp. 546–555 (2016)
4. Arrigoni, F., Maset, E., Fusiello, A.: Synchronization in the symmetric inverse semigroup. In: International Conference on Image Analysis and Processing, pp. 70–81. Springer (2017)
5. Arrigoni, F., Rossi, B., Fusiello, A.: Spectral synchronization of multiple views in SE(3). SIAM Journal on Imaging Sciences **9**(4), 1963 – 1990 (2016)

6. Barazzetti, L., Scaioni, M., Gianinetto, M.: Automatic co-registration of satellite time series via least squares adjustment. European Journal of Remote Sensing **47**(1), 55–74 (2014)
7. Bernard, F., Thunberg, J., Gemmar, P., Hertel, F., Husch, A., Goncalves, J.: A solution for multi-alignment by transformation synchronisation. In: Proc. of the IEEE Conf. on Computer Vision and Pattern Recognition, pp. 2161–2169 (2015)
8. ESA: Sentinel Hub. https://www.sentinel-hub.com. Accessed on 19 February 2020
9. ESA: Sentinel online. https://earth.esa.int/web/sentinel/technical-guides/sentinel-2-msi/performance. Accessed on 19 February 2020
10. European Commission (EC): DIAS. https://www.copernicus.eu/en/access-data/dias. Accessed on 19 February 2020
11. European Commission (EC): Copernicus sentinel data access 2018 annual report. https://scihub.copernicus.eu/twiki/pub/SciHubWebPortal/AnnualReport2018/COPE-SERCO-RP-19-0389_-_Sentinel_Data_Access_Annual_Report_Y2018_v1.0.pdf (2018). Accessed on 19 February 2020
12. Förstner, W.: Generic estimation procedures for orientation with minimum and redundant information. In: Calibration and Orientation of Cameras in Computer Vision, pp. 63–94. Springer Verlag: Berlin Heidelberg (2001)
13. Gianinetto, M.: Automatic co-registration of satellite time series. The Photogrammetric Record **27**(140), 462–470 (2012)
14. Gianinetto, M., Barazzetti, L., Dini, L., Fusiello, A., Toldo, R.: Geometric registration of remotely sensed data with samir. In: Third Int. Conf. on Remote Sensing and Geoinformation of the Environment, vol. 9535, p. 95350Q (2015)
15. Gianinetto, M., Scaioni, M.: Automated geometric correction of high-resolution pushbroom satellite data. Photogrammetric Engineering & Remote Sensing **74**(1), 107–116 (2008)
16. Goshtasby, A.A.: 2-D and 3-D image registration: for medical, remote sensing, and industrial applications. John Wiley & Sons: Hoboken, NJ, USA (2005)
17. Lindeberg, T.: Feature detection with automatic scale selection. International Journal of Computer Vision **30**, 79–116 (1998)
18. Roy, D.P., Huang, H., Boschetti, L., Giglio, L., Yan, L., Zhang, H.H., Li, Z.: Landsat-8 and Sentinel-2 burned area mapping - a combined sensor multi-temporal change detection approach. Remote Sensing of Environment **231**, 111,254 (2019)
19. Santellani, E., Maset, E., Fusiello, A.: Seamless image mosaicking via synchronization. ISPRS Annals **IV-2**, 247–254 (2018)
20. Scaioni, M., Barazzetti, L., Gianinetto, M.: Multi-image robust alignment of medium-resolution satellite imagery. Remote Sensing **10**(12), 1969 (2018)
21. Schroeder, P., Bartoli, A., Georgel, P., Navab, N.: Closed-form solutions to multiple-view homography estimation. In: Applications of Computer Vision (WACV), 2011 IEEE Workshop on, pp. 650–657 (2011)
22. Singer, A.: Angular synchronization by eigenvectors and semidefinite programming. Applied and Computational Harmonic Analysis **30**(1), 20 – 36 (2011)
23. Stumpf, A., Michéa, D., Malet, J.P.: Improved co-registration of Sentinel-2 and Landsat-8 imagery for earth surface motion measurements. Remote Sensing **10**(2), 160 (2018)
24. Toldo, R., Gherardi, R., Farenzena, M., Fusiello, A.: Hierarchical structure-and-motion recovery from uncalibrated images. Computer Vision and Image Understanding **140**, 127 – 143 (2015). DOI 10.1016/j.cviu.2015.05.011
25. USGS: Landsat Collection 1. https://www.usgs.gov/land-resources/nli/landsat/landsat-collection-1?qt-science_support_page_related_con=1#qt-science_support_page_related_con. Accessed on 19 February 2020